Article

Differential Effects of the Zn–His–Bkb vs Zn–His–[Asp/Glu] Triad on Zn-Core Stability and Reactivity

Lin, Yu-ming Lee, and Carmay Lim

J. Am. Chem. Soc., **2005**, 127 (32), 11336-11347• DOI: 10.1021/ja051304u • Publication Date (Web): 20 July 2005

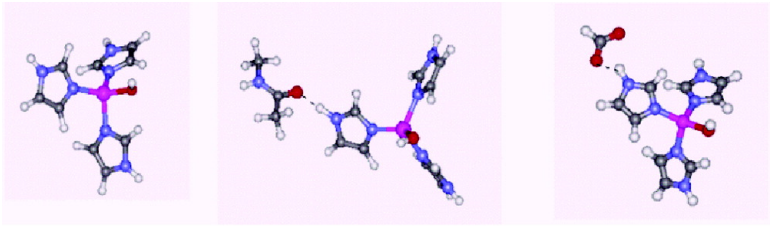

More About This Article

Additional resources and features associated with this article are available within the HTML version:

- Supporting Information
- Links to the 3 articles that cite this article, as of the time of this article download
- Access to high resolution figures
- Links to articles and content related to this article
- Copyright permission to reproduce figures and/or text from this article

View the Full Text HTML

J|A|C|S
ARTICLES
Published on Web 07/20/2005

Differential Effects of the Zn−His−Bkb vs Zn−His−[Asp/Glu] Triad on Zn-Core Stability and Reactivity

Yen-lin Lin,[†] Yu-ming Lee,[†,‡] and Carmay Lim*[,†,‡]

Contribution from the Institute of Biomedical Sciences, Academia Sinica, Taipei 115, Taiwan R.O.C., and Department of Chemistry, National Tsing Hua University, Hsinchu 300, Taiwan R.O.C.

Received March 2, 2005; E-mail: carmay@gate.sinica.edu.tw

Abstract: The most common partner of the Zn-bound His is the Asp/Glu carboxylate side chain in *catalytic* Zn sites and the backbone (Bkb) carbonyl group in *structural* Zn sites. To elucidate the factors governing the selection of the second-shell partner of the Zn-bound His in structural/catalytic Zn sites, systematic studies using density functional theory and continuum dielectric calculations were performed to determine the relative contributions of the second-shell Bkb carbonyl and the Asp/Glu carboxylate to the Zn-core stability and reactivity. The results show that the contributions of the second-shell Bkb carbonyl and Asp/Glu carboxylate to the Zn-core stability depend mainly on the solvent accessibility of the Zn-site and the composition of the Zn-core. They reveal the advantage of a second-shell Bkb carbonyl in *anionic* Zn cavities: it stabilizes *anionic*, *buried* Zn-cores more than the corresponding negatively charged Asp/Glu carboxylate, thus explaining the absence of the Zn−His−Asp/Glu triad in structural $[Zn(Cys)_3(His)]^-$ cores. They also reveal the advantage of a second-shell Asp/Glu carboxylate in *catalytic* Zn-cores: relative to a Bkb carbonyl group, it increases (i) the HOMO energy of the cationic/neutral zinc core, (ii) the reactivity of the attacking Zn-bound OH^-, (iii) electron transfer to the substrate, and (iv) the stability of the metal complex upon electron transfer. Furthermore, a second-shell Asp/Glu carboxylate could facilitate product release in the common *cationic* catalytic cores, by acting as a proton acceptor of the Zn-bound His creating an Asp···His^- dyad that stabilizes the zinc dication more than the respective Bkb···His^0 dyad.

Introduction

Zn^{2+}, the second-most abundant transition metal in humans,[1] can play either a catalytic and/or structural role in proteins.[2−19] In structural Zn sites, Zn^{2+} plays an essential role in maintaining the structural stability of the protein. The most common structural Zn sites are found in proteins involved in nucleic acid binding and gene regulation, belonging to the Zn-finger family, where Zn^{2+} does not directly mediate protein−nucleic acid interaction but induces the correct folding of Zn-finger proteins and stabilizes the active conformation for interaction with the nucleic acid. Apart from playing a structural role, Zn^{2+} can also play a regulatory role in electron transfer, substrate oxidation−reduction, and transport processes. Furthermore, Zn^{2+} can play a catalytic role in (i) facilitating the ionization of a first-shell water molecule to a nucleophilic hydroxide ion in proteins[20] such as carbonic anhydrase[21,22] and metallo-β-lactamase[23] or (ii) stabilizing the negatively charged intermediate of enzymes such as carboxypeptidase A[24,25] and alcohol dehydrogenase.[26,27]

Interestingly, a survey of Zn-proteins in the Protein Data Bank[28,29] (PDB) has shown that catalytic and structural zinc

[†] Academia Sinica.
[‡] National Tsing Hua University.

(1) Sun, G.; Budde, R. J. A. *Biochemistry* **1999**, *38*, 5659−5665.
(2) Christianson, D. W.; Alexander, R. S. *J. Am. Chem. Soc.* **1989**, *111*, 6412−6419.
(3) Vallee, B. L.; Auld, D. S. *Biochemistry* **1990**, *29*, 5647−5659.
(4) Christianson, D. W. *Adv. Protein Chem.* **1991**, *42*, 281−355.
(5) Coleman, J. E. *Annu. Rev. Biochem.* **1992**, *61*, 897−946.
(6) Predki, P. F.; Sarkar, B. *J. Biol. Chem.* **1992**, *267*, 5842−5846.
(7) Gockel, P.; Vahrenkamp, H.; Zuberbuhler, A. D. *Helv. Chim. Acta* **1993**, *76*, 511−520.
(8) Schwabe, J. W. R.; Klug, A. *Nat. Struct. Biol.* **1994**, *1*, 345−349.
(9) Ippolito, J. A.; Baird, T. T.; McGee, S. A.; Christianson, D. W.; Fierke, C. A. *Proc. Natl. Acad. Sci. U.S.A.* **1995**, *92*, 5017−5021.
(10) Kiefer, L. L.; Paterno, S. A.; Fierke, C. A. *J. Am. Chem. Soc.* **1995**, *117*, 6831−6837.
(11) Gockel, P.; Vahrenkamp, H. *Chem. Ber.* **1996**, *129*, 1243−1249.
(12) Lipscomb, W. N.; Strater, N. *Chem. Rev.* **1996**, *96*, 2375−2433.
(13) Karlin, S.; Zhu, Z.-Y. *Proc. Natl. Acad. Sci. U.S.A.* **1997**, *94*, 14231−14236.
(14) Alberts, I. L.; Nadassy, K.; Wodak, S. J. *Protein Sci.* **1998**, *7*, 1700−1716.
(15) Dudev, T.; Lim, C. *Chem. Rev.* **2003**, *103*, 773−787.
(16) Cox, E. H.; Hunt, J. A.; Compher, K. M.; Fierke, C. A.; Christianson, D. W. *Biochemistry* **2000**, *39*, 13687−13694.
(17) McCall, K. A.; Huang, C.-C.; Fierke, C. A. *J. Nutr.* **2000**, *130*, 1437S−1446S.
(18) Laity, J. H.; Lee, B. M.; Wright, P. E. *Curr. Opin. Struct. Biol.* **2001**, *11*, 39−46.
(19) Dudev, T.; Lin, Y. L.; Dudev, M.; Lim, C. *J. Am. Chem. Soc.* **2003**, *125*, 3168−3180.
(20) Eriksson, E.; Liljas, A. *J. Biol. Chem.* **1986**, *261*, 16247−16248.
(21) Silverman, D. N.; Lindskog, S. *Acc. Chem. Res.* **1988**, *21*, 30−36.
(22) Christianson, D. W.; Cox, J. D. *Annu. Rev. Biochem.* **1999**, *68*, 33−57.
(23) Parkin, G. *Chem. Rev.* **2004**, *104*, 699−768.
(24) Phillips, M.; Fletterick, R.; Rutter, W. *J. Biol. Chem.* **1990**, *265*, 20692−20698.
(25) Christianson, D. W.; Libscomb, W. N. *Acc. Chem. Res.* **1989**, *22*, 62−69.
(26) Kovar, J.; Matyska, L.; Zeppezauer, M.; Maret, W. *Eur. J. Biochem.* **1986**, *155*, 391−396.
(27) Cho, H.; Ramaswamy, S.; Plapp, B. V. *Biochemistry* **1997**, *36*, 382−389.
(28) Bernstein, F. C.; Koetzle, T. F.; Williams, G. J. B.; Meyer, E. F.; Brice, M. D.; Rodgers, J. R.; Kennard, O.; Shimanouchi, T.; Tasumi, M. *J. Mol. Biol.* **1977**, *122*, 535−542.
(29) Berman, H. M. et al. *Acta Crystallogr., Sect. D* **2002**, *58*, 899−907.

10.1021/ja051304u CCC: $30.25

sites exhibit distinct first- and second-shell ligand distributions.[19] In "catalytic" Zn sites, His is found bound to Zn^{2+} roughly seven times more often than Cys, whereas, in "structural" Zn sites, it occurs less than half as often as Cys.[19] Catalytic and structural Zn sites also differ in the frequency distribution of the *second-shell* partner of the Zn-bound His. The Asp/Glu carboxylate side chain is the most common partner of the Zn-bound His in *catalytic* zinc sites, but it is seldom the Zn-bound His partner in structural Zn sites; instead, the backbone (Bkb) carbonyl group is the most common partner of the Zn-bound His in *structura*l sites.[19] Consistent with the ubiquitous presence of the Zn−His−Asp/Glu and Zn−His−Bkb (denoted by Zn−His−[Asp/Glu, Bkb]) triads in catalytic and structural Zn sites, respectively, electrostatic potential calculations show that the *enzymatic* Zn-cores of cytidine deaminase and liver alcohol dehydrogenase are negatively screened and contain fewer Zn−[Cys,His]−Bkb hydrogen bonds than structural Zn-cores.[30] These results indicate that the structural or catalytic functions of Zn^{2+} can be distinguished by the different Zn-cores and their immediate surroundings. They also suggest that the Zn−His−[Asp/Glu, Bkb] triads play different roles in maintaining protein structure and/or function.[2]

Several functions of the Zn−His−[Asp/Glu, Bkb] triad have been proposed. Hydrogen bonds to the Zn-bound His are assumed to play an important structural role in properly orienting the metal ligands.[31] The second-shell Asp/Glu in the Zn−His−Asp/Glu triad has been shown to increase the negative charge of its partner, His, thus creating an anionic hole that can electronically enhance metal complexation, provided that the Zn-complex is cationic/neutral and buried.[32] Furthermore, it can modulate the ionization state of the Zn-bound His by acting as either a hydrogen bond or proton acceptor of the Zn-bound His, depending on the electronic properties of the other Zn-ligands and the solvent accessibility of the Zn-site.[32] It can also facilitate the deprotonation of the Zn-bound water at pH > 7 if the Zn-site is solvent exposed.[2,32] Notably, the Zn−His−Asp/Glu triad is found in enzymes of different origins and different functions, suggesting that it may serve a common function in catalysis.[2]

Although the aforementioned functions have been proposed for the Zn−His−[Bkb,Asp/Glu] triads in proteins, the differences in the roles of the Bkb carbonyl and the Asp/Glu carboxylate, the most common partner of Zn-bound His in structural and catalytic sites, respectively, remain unclear. For example, if both the Bkb carbonyl and the Asp/Glu carboxylate could play a structural role in hydrogen bonding to the Zn-bound His (see above), then why is the Zn−His−Asp/Glu triad seldom observed[19] in structural Zn-sites? In other words, what is the difference between the Bkb carbonyl and the Asp/Glu carboxylate in stabilizing structural/catalytic Zn-cores of various compositions? Along the same vein, what is the difference between the Zn−His−Bkb vs the Zn−His−Asp/Glu triad in affecting the reactivity of catalytic Zn sites during the course of the enzyme-catalyzed reaction?

To address these questions, we modeled Zn-cores of various compositions, including the three most common types of catalytic Zn-cores with the Zn-bound water either neutral or deprotonated; viz., (1) [Zn (H_2O/OH^-) ($His)_3$], (2) [Zn (H_2O/OH^-) (Asp/Glu) ($His)_2$], and (3) [Zn (H_2O/OH^-) ($Cys)_2$ (His)]. The latter three types of Zn-complexes were used in modeling the enzymatic reaction between human carbonic anhydrase II and CO_2, carboxypeptidase A and the peptide Bkb, as well as liver alcohol dehydrogenase and alcohol, respectively (see Figure 1). To determine the difference between the second-shell Bkb carbonyl and the Asp/Glu carboxylate in stabilizing Zn-cores of various compositions, we computed the free energies for replacing an outer-shell water molecule with an Asp/Glu carboxylate and a Bkb carbonyl in model Zn-complexes using a combination of ab initio and continuum dielectric methods. To determine the different effects of the Zn−His−Bkb vs the Zn−His−Asp/Glu triad on the reactivity of catalytic Zn-cores during the course of the enzyme-catalyzed reaction, we evaluated the difference between the second-shell Bkb carbonyl and the Asp/Glu carboxylate in facilitating (i) the Zn-bound hydroxide attack of electrophilic substrates and (ii) product release. For the former (i), we computed global/local reactivity descriptors

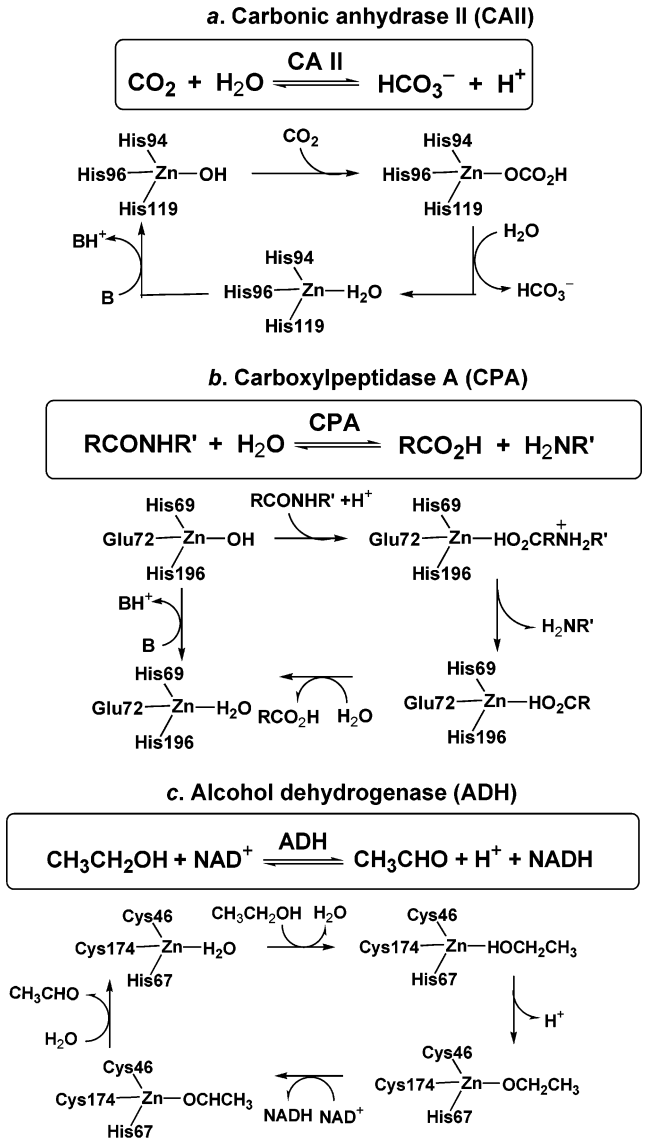

Figure 1. Mechanistic schemes for (a) the hydration of carbon dioxide by carbonic anhydrase II (CAII), (b) the hydrolysis of the peptide bond by carboxypeptidase A (CPA), and (c) the NAD^+-dependent conversion of primary alcohols to aldehydes by alcohol dehydrogenase (ADH). His 119 in (a), His 69 in (b), and His 67 in (c) participate in the catalytic triad.

(30) Maynard, A. T.; Covell, D. G. *J. Am. Chem. Soc.* **2001**, *123*, 1047−1058.
(31) Kester, W. R.; Matthews, B. W. *J Biol. Chem.* **1977**, *252*, 7704−7710.
(32) Lin, Y.-L.; Lim, C. *J. Am. Chem. Soc.* **2004**, *126*, 2602−2612.

such as hardness and Fukui functions[33] (see next section), which have been successfully used in predicting and interpreting the reactivity of various types of electrophilic and nucleophilic reactions,[34−36] while, for the latter (ii), we calculated the free energies for displacing a Zn-bound product by a water molecule in representative catalytic Zn-cores (see Figure 1). The results described herein elucidate the biological significance of the Zn−His−Bkb and Zn−His−Asp/Glu triads and their functional differences in zinc-essential proteins.

Theoretical Background

Global Reactivity Indices. The electronic chemical potential (μ) and absolute hardness (η)[37] measure the total electronic energy, E, response of a molecule of N electrons to electron transfer and redistribution during a chemical reaction. The change in the electronic energy upon electron transfer is μ, the negative of the electronegativity, χ; i.e.,

$$\mu = -\chi = \left(\frac{\partial E}{\partial N}\right)_{v(r)} \cong -\left(\frac{\mathrm{IE} + \mathrm{EA}}{2}\right) \tag{1}$$

where $v(\mathbf{r})$ is the potential energy acting on an electron at $\mathbf{r}$ due to all nuclei. By finite-difference approximation of $(\partial E/\partial N)_{v(r)}$, μ can be estimated from the molecule's ionization energy (IE, the energy associated with the ground-state removal of an electron) and electron affinity (EA, the energy associated with the ground-state addition of an electron). The chemical potential, μ, of the electrons (or electronegativity χ) measures the escaping tendency of the electrons from the molecule and is constant everywhere for an equilibrium system.[37]

The first derivative of the electronic chemical potential or the second derivative of the electronic energy with respect to N is the absolute/global hardness of a molecule:

$$\eta = \frac{1}{2}\left(\frac{\partial \mu}{\partial N}\right)_{v(r)} = \frac{1}{2}\left(\frac{\partial^2 E}{\partial N^2}\right)_{v(r)} \cong \frac{\mathrm{IE} - \mathrm{EA}}{2} \tag{2}$$

By finite-difference approximation of $(\partial^2 E/\partial N^2)_{v(r)}$, η can be estimated from the difference between the ionization energy and the electron affinity, which correspond, respectively, to energies of the highest occupied molecular orbital (HOMO) and the lowest unoccupied molecular orbital (LUMO). Thus, hard molecules (with large η) have a large HOMO−LUMO energy gap and resist deformation/charge redistribution. The inverse of η is global softness (S), which determines how easily electrons are polarized:

$$S = \frac{1}{2\eta} = \left(\frac{\partial N}{\partial \mu}\right)_{v(r)} = \frac{1}{(\mathrm{IE} - \mathrm{EA})} \tag{3}$$

When an electron acceptor (A) and donor (B) react, electrons will flow from the molecule of high μ_B^0 (low electronegativity) to that of lower μ_A^0 (higher electronegativity) until the electronic chemical potentials of A and B become equal ($\mu_A = \mu_B$)[37,38] and the product AB is formed. The approximate number of electrons transferred from B to A, ΔN, in the donor−acceptor reaction is, to first-order, proportional to the original chemical potential difference, $\mu_B^0 - \mu_A^0$, and is given by

$$\Delta N = \frac{1}{2}\frac{\mu_B^0 - \mu_A^0}{\eta_A + \eta_B} \tag{4}$$

Equation 4 shows that electron transfer depends only on the properties of the isolated reactant molecules. It is driven by the electronic chemical potential/electronegativity difference between A and B as well as the global softness of the reactants.[39] Electron-transfer results in a net stabilization (lowering of energy), which is given by

$$\Delta E = -\frac{1}{4}\frac{(\mu_B^0 - \mu_A^0)^2}{\eta_A + \eta_B} \tag{5}$$

Local Reactivity Indices. Unlike μ and χ, which are global quantities characterizing the molecule as a whole, S need not be constant and can have local values. Local softness is defined in terms of the *local* change in the electron density (ρ) at a given site $\mathbf{r}$ of a molecule upon a *global* change in its electronic chemical potential:[40]

$$s(\mathbf{r}) = \left(\frac{\partial \rho(\mathbf{r})}{\partial \mu}\right)_{v(\mathrm{r})} \tag{6}$$

such that

$$\int s(\mathbf{r})\, \mathrm{d}\mathbf{r} = S \tag{7}$$

The local softness, $s(\mathbf{r})$, can be rewritten as

$$s(\mathbf{r}) = \left(\frac{\partial \rho(\mathbf{r})}{\partial N}\right)_v \left(\frac{\partial N}{\partial \mu}\right)_v = f(\mathbf{r}) \cdot \mathbf{S} \tag{8}$$

where $f(\mathbf{r})$ is the Fukui/frontier function,[33] defined as the change in electron density $\rho(\mathbf{r})$ due to a change in the number of electrons N. Both $s(\mathbf{r})$ and $f(\mathbf{r})$ probe the reactivity of different sites within a molecule, differentiating reactivity at one part of a molecule from another. Electron transfer occurs easiest at the site with the largest local softness/charge delocalization.

When the molecule is donating electrons,

$$f^-(\mathbf{r}) = \left(\frac{\partial \rho(\mathbf{r})}{\partial N}\right)_v \cong \rho_{\mathrm{HOMO}}(\mathbf{r}) \tag{9}$$

measures reactivity of a site toward an electrophilic reagent (e.g., H^+). The Fukui function, $f^-(\mathbf{r})$, can be redefined to reflect the reactivity of different atoms (as opposed to different sites) within a molecule by estimating it in terms of the change in the charge of an atom, k, in a molecule with N electrons upon adding or removing an electron:[34]

$$f_k^- = q_k(N) - q_k(N-1) \tag{10}$$

where $q_k(N)$ and $q_k(N-1)$ represent the electronic population of atom k in a molecule with N and $N-1$ electrons, respectively.

(33) Parr, R. G.; Yang, W. *J. Am. Chem. Soc.* **1984**, *106*, 4049−4050.
(34) Yang, W.; Mortier, W. J. *J. Am. Chem. Soc.* **1986**, *108*, 5708−5711.
(35) Maynard, A. T.; Huang, M.; Rice, W. G.; Covell, D. G. *Proc. Natl. Acad. Sci. U.S.A.* **1998**, *95*, 11578−11583.
(36) Chen, H.-T.; Ho, J.-J. *J. Phys. Chem. A* **2003**, *107*, 7643−7649.
(37) Parr, R. G.; Pearson, R. G. *J. Am. Chem. Soc.* **1983**, *105*, 7512−7516.
(38) Sanderson, R. T. *Polar Covalence*; Academic: New York, 1983.
(39) Pearson, R. G. *Inorg. Chem.* **1988**, *27*, 734−740.
(40) Yang, W.; Parr, R. G. *Proc. Natl. Acad. Sci. U.S.A.* **1985**, *82*, 6723−6726.

Table 1. Comparison between Computed and Experimental CO_2 and $HCONH_2$ Reactivity Indices (eV)[a]

	CO_2				$HCONH_2$			
method	EA (eV)	IE (eV)	μ (eV)	η (eV)	EA (eV)	IE (eV)	μ (eV)	η (eV)
experiment[b]	−3.8	13.8	−5.0	8.8	−2.0	10.3	−4.2	6.2
eq 12, MP2/6-31+G(d)[c]	−1.5	14.8	−6.7	8.2	−1.8	11.5	−4.8	6.6
eq 12, MP3/6-31+G(d)[c]	−1.5	14.9	−6.7	8.2	−1.8	11.5	−4.8	6.6
eq 12, MP2/6-311++G(d,p)[c]	−1.5	14.9	−6.7	8.2	−0.9	11.5	−5.3	6.2
eq 12, S-VWN/6-31+G(d)	1.4	9.8	−5.6	4.2	1.4	6.6	−4.0	2.6
eq 12, SVWN/6-311++G(d,p)[c]	1.4	9.9	−5.6	4.2	1.5	6.7	−4.1	2.6
eq 12, B3LYP/6-31+G(d)[c]	0.6	10.5	−5.5	5.0	0.2	7.4	−3.8	3.6
eq 12, B3LYP/6-311++G(d,p)[c]	0.6	10.5	−5.5	5.0	0.6	7.4	−4.0	3.4
eq 12, B3-P86/6-31+G(d)[c]	0.7	11.1	−5.9	5.2	0.4	7.9	−4.1	3.8
eq 12, B-VWN/6-31+G(d)[c]	1.5	9.9	−5.7	4.2	1.4	6.9	−4.2	2.7
eq 12, B3-PW91/6-31+G(d)[c]	0.2	10.5	−5.4	5.1	−0.1	7.4	−3.6	3.8
eq 13, MP2/6-31+G(d)[d]	2.6	14.5	−8.5	6.0	1.5	11.1	−6.3	4.8
eq 13, MP3/6-31+G(d)[d]	2.5	13.8	−8.2	5.6	1.5	10.6	−6.0	4.5
eq 13, S-VWN/6-31+G(d)	0.4	14.6	−7.5	7.1	0.6	10.8	−5.7	5.1
eq 13, B3LYP/6-31+G(d)[d]	0.9	13.8	−7.4	6.5	1.2	10.7	−5.9	4.8

[a] Based on S-VWN/6-31+G(d) geometries. [b] From Pearson, 1988.[39] [c] Based on single-point calculations using eq 12a for EA, eq 12b for IE, eq 1 for μ, and eq 2 for η. [d] Based single-point calculations using eq 13a for EA, eq 13b for IE, eq 1 for μ, and eq 2 for η.

Using eqs 8 and 10, the local softness for atom k can be written as

$$s_k^- = [q_k(N) - q_k(N-1)] \times S \tag{11}$$

Calculations

Models Used. We modeled the common catalytic and structural Zn− sites in proteins containing the Zn−His−[Asp/Glu, Bkb] triad;[14] viz., [Zn (H_2O/OH) ($His)_3$], [Zn (H_2O/OH) (Asp/Glu) ($His)_2$], and [Zn (H_2O/OH) ($Cys)_2$ (His)] for catalytic cores and [Zn ($Cys)_2$ ($His)_2$] and [Zn ($Cys)_3$ His] for structural cores. The side chains of histidine, aspartic acid/glutamic acid, and cysteine were modeled by imidazole/imidazolate (ImH/Im^-), formic acid/formate ($HCOOH/HCOO^-$), and methyl thiolate (CH_3S^-), respectively, while the backbone peptide group was modeled by $CH_3CONHCH_3$.

Geometry Optimization. In our previous studies[32,41] we had shown that the S-VWN/6-31+G(d) method is suitable for evaluating the geometries of complexes between Zn^{2+} and oxygen-/nitrogen-/sulfur-containing ligands. Consequently, *full* (unless stated otherwise) geometry optimization for each metal complex studied was carried out at the S-VWN/6-31+G(d) level using the Gaussian 03 program.[42] S-VWN/6-31+G(d) vibrational frequencies were then computed to verify that each complex was at the minimum of its potential energy surface. No imaginary frequency was found in any of the fully optimized complexes.

Reactivity Index Calculations. To determine the optimal method for computing global reactivity descriptors (see above section) we compared the experimental electron affinity (EA), ionization energy (IE), chemical potential (μ), and hardness (η) of CO_2 and $HCONH_2$ with the respective values computed using various methods (see Table 1). The IE and the EA can be estimated by

$$\mathrm{EA} \approx -E_{\mathrm{elec}}^{\ \mathrm{LUMO}} \tag{12a}$$

$$\mathrm{IE} \approx -E_{\mathrm{elec}}^{\ \mathrm{HOMO}} \tag{12b}$$

or by

$$\mathrm{EA} \approx E_{\mathrm{elec}}(N+1) - E_{\mathrm{elec}}(N) \tag{13a}$$

$$\mathrm{IE} \approx E_{\mathrm{elec}}(N-1) - E_{\mathrm{elec}}(N) \tag{13b}$$

where $E_{\mathrm{elec}}(N+1)$, $E_{\mathrm{elec}}(N)$, and $E_{\mathrm{elec}}(N-1)$ represent the electronic energies of molecules with $N+1$, N, and $N-1$ electrons, respectively.

Scheme 1

$$\begin{array}{ccc} & \xrightarrow{\Delta G^1} & \\ \text{Reactants } (\varepsilon = 1) & \rightarrow & \text{Products } (\varepsilon = 1) \\ \Delta G_{\mathrm{solv}}{}^x(\text{Reactants}) \downarrow & & \downarrow \Delta G_{\mathrm{solv}}{}^x(\text{Products}) \\ \text{Reactants } (\varepsilon = x) & \rightarrow & \text{Products } (\varepsilon = x) \\ & \xrightarrow{\Delta G^x} & \end{array}$$

Thus, the EA and IE of CO_2 and $HCONH_2$ were estimated from the computed electronic energies using eq 12 or 13 based on fully optimized S-VWN/6-31+G(d) geometries, while the corresponding μ and η were estimated from the EA and IE values using eqs 1 and 2, respectively.

Table 1 compares the experimental EA, IE, μ, and η values of CO_2 and $HCONH_2$ with those computed at various theory/basis set levels using S-VWN/6-31+G(d) geometries. Although not shown, the reactivity indices in Table 1 are only negligibly perturbed if the geometries were optimized with different methods. Table 1 shows that MP2 calculations using eq 12 yielded the closest overall agreement with the respective measured values, whereas the corresponding DFT calculations using eq 12 or calculations based on eq 13 yielded generally positive EA values of CO_2 and $HCONH_2$, opposite in sign to the experimental numbers. Neither MP3 nor a larger 6-311++G(d,p) basis set improved the MP2/6-31+G(d)//S-VWN/6-31+G(d) results based on eq 12 (see Table 1). Therefore, all the global reactivity descriptors (eqs 1−5) in this work were estimated at the MP2/6-31+G(d)//S-VWN/6-31+G(d) level using eq 12, while the local reactivity descriptors (eqs 10 and 11) were estimated by carrying out natural population analysis calculations on the N and $N-1$ electron molecules.

Gas-Phase Free Energy Calculations. In our previous studies[32,41] we had calibrated the MP2/6-31+G(d)//S-VWN/6-31+G(d) method with respect to available experimental data and showed that it is suitable for evaluating the gas-phase free energies of complexes between Zn^{2+} and oxygen-/nitrogen-/sulfur-containing ligands. Consequently, the electronic energies E_{elec} were evaluated at the MP2/6-31+G(d)//S-VWN/6-31+G(d) level. The thermal energy (E_T), which includes the zero-point energy[43] and the total entropy (S), were evaluated using standard statistical mechanical formulas[44] after scaling the vibrational frequencies by an empirical factor of 0.9833.[45] The ΔE_{elec}, ΔE_T, ΔPV work term, and ΔS differences between the products and reactants were used to compute the gas-phase free energy, ΔG^1, at room temperature, T = 289.15 K, according to

$$\Delta G^1 = \Delta E_{\mathrm{elec}} + \Delta E_T + \Delta PV - T\Delta S \tag{14}$$

Solvation Free Energy Calculations. The reaction free energy, ΔG^x, in a given environment characterized by a dielectric constant $\epsilon = x$ was calculated according to the thermodynamic cycle shown in Scheme 1.

ΔG^1 is the gas-phase free energy computed using eq 14, while $\Delta G_{\mathrm{solv}}{}^x$ is the free energy for transferring a molecule in the gas phase to a continuous medium characterized by a dielectric constant, x. Thus, the ΔG^x can be computed from

$$\Delta G^x = \Delta G^1 + \Delta G_{\mathrm{solv}}{}^x(\text{Products}) - \Delta G_{\mathrm{solv}}{}^x(\text{Reactants}) \tag{15}$$

$\Delta G_{\mathrm{solv}}{}^x$ was estimated by solving Poisson's equation using finite difference methods.[46,47] The dielectric calculations employed a 71 ×

(41) Dudev, T.; Lim, C. *J. Am. Chem. Soc.* **2002**, *124*, 6759−6766.
(42) Frisch, M. J. et al. *Gaussian 03*, rev. B.03; Gaussian, Inc.: Pittsburgh, PA, 2003.
(43) Foresman, J. B.; Frisch, E. *Exploring Chemistry with Electronic Structure Methods*, 2nd ed.; Gaussian, Inc.: Pittsburgh, PA, 1996.
(44) McQuarrie, D. A. *Statistical Mechanics*; Harper and Row: New York, 1976.
(45) Wong, M. W. *Chem. Phys. Lett.* **1996**, *256*, 391−399.
(46) Gilson, M. K.; Honig, B. *Biopolymers* **1986**, *25*, 2097−2119.
(47) Lim, C.; Bashford, D.; Karplus, M. *J. Phys. Chem.* **1991**, *95*, 5610−5620.

Table 2. Effective Solute Radii for Continuum Dielectric Calculations

compound	$\Delta G_{solv,expt}{}^{80}$ (kcal/mol)	$\Delta G_{solv,calc}{}^{80}$ (kcal/mol)	atom type	R_{eff} (Å)
ImH	−10.2[a]	−10.2	C^{sp2}	2.20
			N^{sp2}	1.97
			H^{C}	1.47
			H^{N}	0.23
$CH_3CONHCH_3$	−10.0[b]	−10.0	C^{sp3}	2.30
			O^{sp2}	1.86
CH_3COOH	−6.7[a]	−6.7	O^{H}	2.14
			H^{O}	0.23
CH_3SH	−1.2[c]	−1.2	S^{H}	2.45
			H^{S}	0.23
H_2O	−6.3[c]	−6.3	O^{H_2O}	2.14
			H^{H_2O}	1.00
CH_3COO^-	−77.7[d]	−77.6	O^{COO-}	1.62
CH_3S^-	−75.9[e]	−75.9	S^-	1.90
Im^-	−60.9[f]	−61.2	N^-	2.26
$[Zn\ W_6]^{2+}$	−221.0[g]	−221.0	Zn^{2+}	1.40
			O^{H_2O}	1.82
			H^{H_2O}	1.00
$[(Zn\ W_3\ OH)\cdot W_2]^+$	−90.6[h]	−90.9	O^{OH-}	1.50
			H^{OH-}	0.23

[a] From Wolfenden et al., 1981.[54] [b] From Wolfenden, 1978.[55] [c] From Hine and Mookerjee, 1975.[56] [d] Using eq 16 with $pK_{a,expt}(CH_3COOH) = 4.8$[57] and $\Delta G_{expt}{}^1(CH_3COOH \rightarrow CH_3COO^- + H^+) = 341.5$ kcal/mol.[58] [e] Using eq 16 with $pK_{a,expt}(CH_3SH) = 10.3$[59] and $\Delta G_{expt}{}^1(CH_3SH \rightarrow CH_3S^- + H^+) = 352.7$ kcal/mol.[58] [f] Using eq 16 with $pK_{a,expt}(ImH) = 14.5$[60] and $\Delta G_{calc}{}^1(ImH \rightarrow Im^- + H^+) = 334.8$ kcal/mol. [g] Using eq 17 with $\Delta G_{solv,expt}{}^{80}(Zn^{2+}) = -484.6$ kcal/mol,[51] and $\Delta G_{calc}{}^1(Zn^{2+} + 6W \rightarrow [Zn\ W_6]^{2+}) = -263.6$ kcal/mol. [h] Using eq 16 with $pK_{a,expt}([Zn\ W_6]^{2+}) = 9.0$[53] and $\Delta G_{calc}{}^1([Zn\ W_6]^{2+} \rightarrow \{[Zn\ W_3\ OH]\cdot W_2\}^+ + H^+) = 145.8$ kcal/mol.

71 × 71 lattice with a final grid spacing of 0.25 Å, ab initio geometries, and natural bond orbital (NBO) atomic charges.[48] The low-dielectric region of the solute was defined as the region inaccessible to contact by a 1.4-Å-radius sphere rolling over the molecular surface, which was defined by the effective solute radii, R_{eff}, listed in Table 2. This region was assigned an internal dielectric constant ϵ_{in} of 2 to account for the electronic polarizability of the solute. Poisson's equation was then solved with $\epsilon_{in} = 2$ and ϵ_{out} equal to 2, 4, 20, or 80, representing Zn sites of increasing solvent exposure. The difference between the computed electrostatic potential in a given dielectric medium ($\epsilon_{out} = x$) and that in the gas phase ($\epsilon_{out} = 1$) yielded the solvation free energy $\Delta G_{solv}{}^x$.

Determining the Effective Dielectric Boundary for Solvation Free Energy Calculations. The effective radii, R_{eff}, for the various atoms listed in Table 2 were obtained by adjusting the CHARMM (version 22)[49] van der Waals radii to reproduce the experimental hydration free energies as well as the absolute and relative pK_a values of the model compounds and the metal complexes. First, the CHARMM van der Waals radii of sp^3 carbon (C^{sp3}), sp^2 carbon (C^{sp2}), sp^2 nitrogen (N^{sp2}), water oxygen (O^{H_2O}), hydroxyl oxygen (O^H), sp^2 oxygen (O^{sp2}), thiol sulfur (S^H), H^C, H^N, H^{H_2O}, H^O, and H^S were simultaneously adjusted to reproduce the experimental hydration free energies of ImH, $CH_3CONHCH_3$, CH_3COOH, CH_3SH, and water (see Table 2).

Next, the radii of the carboxylate oxygen (O^{COO-}), thiolate sulfur (S^-), and imidazolate nitrogen (N^-) were simultaneously adjusted to reproduce the measured absolute as well as relative pK_a values of CH_3COOH, CH_3SH, and ImH, which indirectly determine the respective "experimental" hydration free energy of the deprotonated molecule as follows:

$$\Delta G_{solv,expt}{}^{80}(A^-) = \Delta G_{solv,expt}{}^{80}(AH) - \Delta G_{solv,expt}{}^{80}(H^+) + 2.303RT\,pK_{a,expt}(AH) - \Delta G_{expt}{}^1(AH) \quad (16)$$

In eq 16, $A^- = CH_3COO^-$, CH_3S^-, or Im^-; $\Delta G_{solv,expt}{}^{80}(AH)$ is the experimental hydration free energy of the protonated molecule, AH, listed in Table 2; $\Delta G_{solv,expt}{}^{80}(H^+)$ is the experimental proton hydration free energy (−264.0 kcal/mol[50]), $pK_{a,expt}(AH)$ is the measured solution pK_a of AH, and $\Delta G_{expt}{}^1(AH)$ is the experimental gas-phase free energy for deprotonating AH to A^- and H^+ (see Table 2 footnotes). In the case of $ImH \rightarrow Im^- + H^+$, the experimental gas-phase free energy is not available, thus $\Delta G^1(AH)$ was estimated using eq 14 with ΔE_{elec} evaluated at the MP2/6-31+G(d)//S-VWN/6-31+G(d) level (see Table 2 footnotes).

The Zn^{2+} and water (W) oxygen and hydrogen radii were simultaneously adjusted to reproduce the "experimental" hydration free energy of $[Zn\ W_6]^{2+}$, which was estimated from the measured hydration free energy of Zn^{2+} (−484.6 kcal/mol)[51] and the computed gas-phase free energy for $Zn^{2+} + 6W \rightarrow [Zn\ W_6]^{2+}$; i.e.,

$$\Delta G_{solv,expt}{}^{80}([Zn\ W_6]^{2+}) \approx \Delta G_{solv,expt}{}^{80}(Zn^{2+}) - \Delta G_{calc}{}^1(Zn^{2+} + 6W \rightarrow [Zn\ W_6]^{2+}) \quad (17)$$

As basis set superposition error is likely to be significant in complex formation reactions, a counterpoise correction (29.2 kcal/mol) was applied to the gas-phase binding *energy* ΔE_{elec} (−327.7 kcal/mol, evaluated at the MP2/6-31+G(d)//S-VWN/6-31+G(d) level) for $Zn^{2+} + 6W \rightarrow [Zn\ W_6]^{2+}$. The resulting gas-phase *free energy* $\Delta G_{calc}{}^1$ was estimated to be equal to −263.6 kcal/mol.

Our previous work[52] showed that Zn^{2+} changes its coordination number upon deprotonating a Zn-bound water molecule as the hexacoordinated $[Zn\ W_5\ OH]^+$ complex spontaneously decomposed into a tetrahedral $[(Zn\ W_3\ OH)\cdot W_2]^+$ complex with two water molecules in the outer sphere; i.e., $[Zn\ W_6]^{2+} \rightarrow [(Zn\ W_3\ OH)\cdot W_2]^+ + H^+$. Thus, the radii for the Zn-bound hydroxide atoms were simultaneously adjusted to reproduce the "experimental" hydration free energy of $[(Zn\ W_3\ OH)\cdot W_2]^+$, which was estimated from eq 16 with $AH = [Zn\ W_6]^{2+}$, using the "experimental" hydration free energy of $[Zn\ W_6]^{2+}$ (−221.0 kcal/mol), the measured pK_a of $[Zn\ W_6]^{2+}$ (9.0),[53] and the computed gas-phase free energy for deprotonating $[Zn\ W_6]^{2+}$ to $[(Zn\ W_3\ OH)\cdot W_2]^+$ and H^+ (145.8 kcal/mol).

Results

In interpreting the results below, we emphasize the *trend* of the energy/free energy change between *two* sets of reactions so that systematic errors in the computed numbers for the two reactions are likely to cancel. In addition, we have calibrated the calculations against available pertinent experimental data. Errors in the computed geometries and gas-phase free energies have been minimized by calibrating the methods and basis sets employed,[32] while errors in the hydration free energies, $\Delta G_{solv}{}^{80}$, have been minimized by using effective atomic radii that have been adjusted to reproduce the experimental data of the model compounds and the Zn-complexes in aqueous solution (Table 2). These effective radii implicitly take into account the ambiguity in the atomic charges and thus the geometry in solution as well as the neglect of nonelectrostatic forces in computing $\Delta G_{solv}{}^{80}$.

Contributions of the Second-Shell Asp/Glu Carboxylate Relative to the Bkb Carbonyl to the Zn−Core Stability. To

(48) Reed, A. E.; Curtiss, L. A.; Weinhold, F. *Chem. Rev.* **1988**, *88*, 899−926.
(49) Brooks, B. R.; Bruccoleri, R. E.; Olafson, B. D.; States, D. J.; Swaminathan, S.; Karplus, M. *J. Comput. Chem.* **1983**, *4*, 187−217.
(50) Tissandier, M. D.; Cowen, K. A.; Feng, W. Y.; Gundlach, E.; Cohen, M. H.; Earhart, A. D.; Coe, J. V.; Tuttle, T. R., Jr. *J. Phys. Chem. A* **1998**, *102*, 7787−7794.
(51) Burgess, M. A. *Metal ions in solution*; Ellis Horwood: Chichester, U.K., 1978.
(52) Chao, Y. F.; Lim, C. In preparation.
(53) Richens, D. T. *The Chemistry of aqua ions*; John Wiley & Sons: New York, 1997.

Table 3. Free Energies (ΔG^x) for $\{[X]\cdot W\}^m + Y^n \rightarrow \{[X]\cdot Y\}^{m+n} + W$ (W = H_2O) in Model Zinc-Binding Sites Characterized by Dielectric Constant x[a]

rxn	$\{[X]\cdot W\}^m$	Y^n	$\{[X]\cdot Y\}^{m+n} + W$	$\Delta\Delta G^2$	$\Delta\Delta G^4$	$\Delta\Delta G^{20}$	$\Delta\Delta G^{80}$
1a	$\{[Zn\ W\ (ImH)_3]\cdot W\}^{2+}$	$CH_3CONHCH_3$	$\{[Zn\ W\ (ImH)_3]\cdot CH_3CONHCH_3\}^{2+}$	0.0	0.0	0.0	0.0
1b	$\{[Zn\ W\ (ImH)_3]\cdot W\}^{2+}$	$HCOO^-$	$\{[Zn\ W\ (ImH)_2\ Im]\cdot HCOOH\}^+$	−49.9[b]	−13.0[b]	17.6[b]	23.6[b]
2a	$\{[Zn\ W\ HCOO\ (ImH)_2]\cdot W\}^+$	$CH_3CONHCH_3$	$\{[Zn\ W\ HCOO\ (ImH)_2]\cdot CH_3CONHCH_3\}^+$	0.0	0.0	0.0	0.0
2b	$\{[Zn\ W\ HCOO\ (ImH)_2]\cdot W\}^+$	$HCOO^-$	$\{[Zn\ W\ HCOO\ ImH\ Im]\cdot HCOOH\}^0$	−33.9[c]	−10.7[c]	8.7[c]	12.6[c]
3a[d]	$\{[Zn\ W\ CH_3S\ (ImH)_2]\cdot W\}^+$	$CH_3CONHCH_3$	$\{[Zn\ W\ CH_3S\ (ImH)_2]\cdot CH_3CONHCH_3\}^+$	0.0	0.0	0.0	0.0
3b[d]	$\{[Zn\ W\ CH_3S\ (ImH)_2]\cdot W\}^+$	$HCOO^-$	$\{[Zn\ W\ CH_3S\ (ImH)_2]\cdot HCOO\}^0$	−33.1[e]	−12.9[e]	3.1[e]	6.1[e]
4a	$\{[Zn\ W\ (CH_3S)_2\ ImH]\cdot W\}^0$	$CH_3CONHCH_3$	$\{[Zn\ W\ (CH_3S)_2\ ImH]\cdot CH_3CONHCH_3\}^0$	0.0	0.0	0.0	0.0
4b	$\{[Zn\ W\ (CH_3S)_2\ ImH]\cdot W\}^0$	$HCOO^-$	$\{[Zn\ W\ (CH_3S)_2\ ImH]\cdot HCOO\}^-$	−12.8[f]	−4.4[f]	2.7[f]	4.3[f]
5a[d]	$\{[Zn\ OH\ (ImH)_3]\cdot W\}^+$	$CH_3CONHCH_3$	$\{[Zn\ OH\ (ImH)_3]\cdot CH_3CONHCH_3\}^+$	0.0	0.0	0.0	0.0
5b[d]	$\{[Zn\ OH\ (ImH)_3]\cdot W\}^+$	$HCOO^-$	$\{[Zn\ OH\ (ImH)_3]\cdot HCOO\}^0$	−30.5[g]	−10.4[g]	5.7[g]	9.0[g]
6a	$\{[Zn\ OH\ HCOO\ (ImH)_2]\cdot W\}^0$	$CH_3CONHCH_3$	$\{[Zn\ OH\ HCOO\ (ImH)_2]\cdot CH_3CONHCH_3\}^0$	0.0	0.0	0.0	0.0
6b	$\{[Zn\ OH\ HCOO\ (ImH)_2]\cdot W\}^0$	$HCOO^-$	$\{[Zn\ OH\ HCOO\ (ImH)_2]\cdot HCOO\}^-$	−9.5[h]	−2.2[h]	4.0[h]	5.3[h]
7a	$\{[Zn\ OH\ CH_3S\ (ImH)_2]\cdot W\}^0$	$CH_3CONHCH_3$	$\{[Zn\ OH\ CH_3S\ (ImH)_2]\cdot CH_3CONHCH_3\}^0$	0.0	0.0	0.0	0.0
7b	$\{[Zn\ OH\ CH_3S\ (ImH)_2]\cdot W\}^0$	$HCOO^-$	$\{[Zn\ OH\ CH_3S\ (ImH)_2]\cdot HCOO\}^-$	−10.4[i]	−3.6[i]	1.6[i]	2.4[i]
8a	$\{[Zn\ (CH_3S)_2\ (ImH)_2]\cdot W\}^0$	$CH_3CONHCH_3$	$\{[Zn\ (CH_3S)_2\ (ImH)_2]\cdot CH_3CONHCH_3\}^0$	0.0	0.0	0.0	0.0
8b	$\{[Zn\ (CH_3S)_2\ (ImH)_2]\cdot W\}^0$	$HCOO^-$	$\{[Zn\ (CH_3S)_2\ (ImH)_2]\cdot HCOO\}^-$	−12.2[j]	−4.7[j]	1.4[j]	2.5[j]
9a	$\{[Zn\ (CH_3S)_3\ ImH]\cdot W\}^-$	$CH_3CONHCH_3$	$\{[Zn\ (CH_3S)_3\ ImH]\cdot CH_3CONHCH_3\}^-$	0.0	0.0	0.0	0.0
9b	$\{[Zn\ (CH_3S)_3\ ImH]\cdot W\}^-$	$HCOO^-$	$\{[Zn\ (CH_3S)_3\ ImH]\cdot HCOO\}^{2-}$	11.1[k]	1.5[k]	−7.4[k]	−9.3[k]

[a] All energies in kcal/mol; $x = 2$, 4, or 20 represents buried or partially buried zinc-binding sites, whereas $x = 80$ represents fully solvent-exposed sites (see Calculations). [b] Relative to the thermodynamic parameters of reaction 1a, whose ΔG^2, ΔG,[4] ΔG^{20}, and $\Delta G^{80} = -3.1$, −0.3, 1.8, and 2.3 kcal/mol, respectively. [c] Relative to the thermodynamic parameters of reaction 2a, whose ΔG^2, ΔG,[4] ΔG^{20}, and $\Delta G^{80} = -3.7$, −2.4, −1.4, and −1.2 kcal/mol, respectively. [d] Structure optimized with the hydrogen bond distance and angle of the Zn−ImH−[W/$CH_3CONHCH_3$/HCOO] triad restrained to the following values: $R_{N-H} = 1.017$ Å, $R_{H\cdots O} = 2.333$ Å, and the $\theta_{N-H-O} = 150°$; see Lin and Lim (2004), Figures 3a and 4a.[32] [e] Relative to the thermodynamic parameters of reaction 3a, whose ΔG^2, ΔG,[4] ΔG^{20}, and $\Delta G^{80} = -3.5$, −2.3, −1.4, and −1.3 kcal/mol, respectively. [f] Relative to the thermodynamic parameters of reaction 4a, whose ΔG^2, ΔG,[4] ΔG^{20}, and $\Delta G^{80} = 2.1$, 4.1, 6.3, and 6.8 kcal/mol, respectively. [g] Relative to the thermodynamic parameters of reaction 5a, whose ΔG^2, ΔG,[4] ΔG^{20}, and $\Delta G^{80} = -2.5$, −2.1, −2.3, and −2.4 kcal/mol, respectively. [h] Relative to the thermodynamic parameters of reaction 6a, whose ΔG^2, ΔG,[4] ΔG^{20}, and $\Delta G^{80} = 0.3$, 1.3, 2.4, and 2.7 kcal/mol, respectively. [i] Relative to the thermodynamic parameters of reaction 7a, whose ΔG^2, ΔG,[4] ΔG^{20}, and $\Delta G^{80} = -0.8$, 0.02, 1.0, and 1.4 kcal/mol, respectively. [j] Relative to the thermodynamic parameters of reaction 8a, whose ΔG^2, ΔG,[4] ΔG^{20}, and $\Delta G^{80} = 1.4$, 3.2, 4.8, and 5.2 kcal/mol, respectively. [k] Relative to the thermodynamic parameters of reaction 9a, whose ΔG^2, ΔG,[4] ΔG^{20}, and $\Delta G^{80} = -7.8$, −6.1, −4.3, and −3.9 kcal/mol, respectively.

assess the relative contributions of the second-shell Bkb carbonyl and Asp/Glu carboxylate in the Zn−His−[Bkb,Asp/Glu] triad in stabilizing Zn-cores of various compositions, we computed the free energy for replacing an outer-shell water molecule with $HCOO^-$ or $CH_3CONHCH_3$ in $\{[Zn\ (H_2O/OH)\ (L)_k\ (ImH)_l]\cdot H_2O\}^{m+}$ complexes (L = $HCOO^-$ or CH_3S^-; $k = 0-3$; $l = 1-3$; $m = -1$, 0, 1, 2) of varying degrees of solvent exposure. The metal complexes for reactions 1−7 and the last two reactions in Table 3 model, respectively, typical catalytic and structural Zn sites containing the Zn−His−[Bkb,Asp/Glu] triad. Table 3 lists the $H_2O \rightarrow HCOO^-$ exchange free energies relative to the corresponding $H_2O \rightarrow CH_3CONHCH_3$ values; i.e., the free energy change ($\Delta\Delta G_x$) for

$$\{[Zn\ (H_2O/OH)\ (L)_k\ (ImH)_l]\}\cdot CH_3CONHCH_3\}^{m+} + HCOO^- \rightarrow \{[Zn\ (H_2O/OH)\ (L)_k\ (ImH)_l]\}\cdot HCOO\}^{m-1} + CH_3CONHCH_3 \quad (18)$$

Our previous work[32] showed that irrespective of the dielectric medium, the Zn-bound ImH would be deprotonated in the product complexes of reactions 1b and 2b in Table 3 but would remain neutral for the other Zn-complexes. In particular, in the product complexes of reactions 3b and 5b, proton transfer from the Zn-bound His to an outer-shell carboxylate is unlikely to occur in buried or solvent-exposed Zn sites even though it is spontaneous in the gas phase.[32] Thus, the $\{[Zn\ W\ CH_3S\ (ImH)_2]\cdot L\}^m$ and $\{[Zn\ OH\ (ImH)_3]\cdot L\}^m$ (L = H_2O, $CH_3CONHCH_3$, $HCOO^-$; $m = +1$, 0) geometries in reactions 3 and 5 were optimized with constraints (see Table 3, footnotes), and ΔG^1 was approximated by ΔE^1. All the other geometries in Table 3 were *fully* optimized at the S-VWN/6-31+G(d) level. Note that in the *fully* optimized product geometries of reaction 1b, $\{[Zn\ W\ (ImH)_2\ Im]\cdot HCOOH\}^+$, and reaction 2b, $\{[Zn\ W\ HCOO\ ImH\ Im]\cdot HCOOH\}^0$, proton transfer to the outer-shell carboxylate is spontaneous.

(1) Effects of First-Shell Ligands. The results in Table 3 show that, in buried sites, a second-shell $HCOO^-$ stabilizes cationic/neutral Zn-complexes more than the respective $CH_3CONHCH_3$ (negative $\Delta\Delta G^x$, $x \leq 4$, for reactions 1−8), whereas the converse is true for an anionic Zn-complex (positive $\Delta\Delta G^x$, $x \leq 4$, for the last reaction). The degree to which a second-shell $HCOO^-$ stabilizes a Zn-complex relative to a second-shell $CH_3CONHCH_3$ diminishes with decreasing net positive charge of the reactant metal complex: The $|\Delta\Delta G^4|$ for dicationic, monocationic, and neutral Zn-complexes are −13.0, −10.4 to −12.9, and −2.2 to −4.7 kcal/mol, respectively. The observed trend in the $\Delta\Delta G^x$, $x \leq 4$, as a function of the net charge of the reactant Zn-complex reflects the more favorable charge−charge/dipole−charge interactions between a positively charged/neutral metal complex and a negatively charged carboxylate, as compared to the charge−dipole/dipole−dipole interactions between the same metal complex and a neutral carbonyl group in a solvent inaccessible cavity.

(2) Effects of Solvation. As the dielectric constant increases, the $\Delta\Delta G^x$ values for the cationic/neutral metal complexes (Table 3, reactions 1−8) become less negative and become positive when ϵ is ≥20. The positive $\Delta\Delta G^{80}$ in aqueous solution is mainly because the dehydration penalty of $HCOO^-$ (78.4 kcal/mol) is much greater than that of $CH_3CONHCH_3$ (10 kcal/mol, Table 2). In addition, a di- or monocationic Zn-complex with an outer-shell $CH_3CONHCH_3$ is much better solvated than the respective metal complex with one less positive net charge due to an outer-shell $HCOO^-$ (Table 3, reactions 1−3 and 5). In

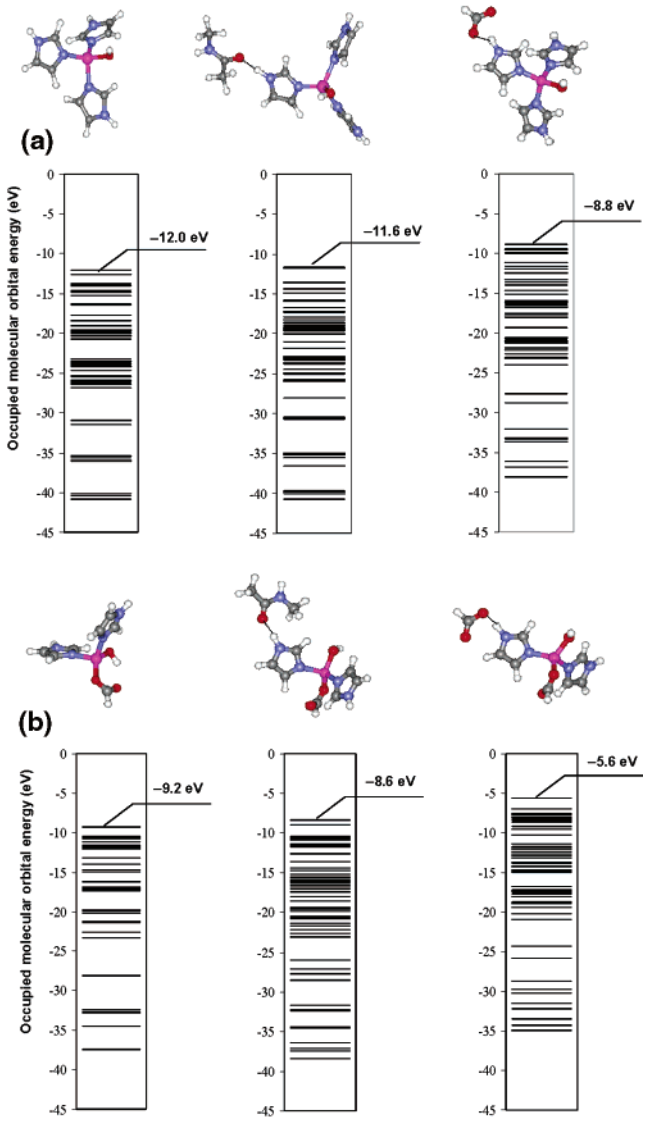

Figure 2. High-energy end of the occupied MO energy spectrum for (a) the $[Zn\ OH\ (ImH)_3]^+$ complex and (b) the $[Zn\ OH\ (HCOO)\ (Im)_2]^0$ complex in the absence and presence of a second-shell $CH_3CONHCH_3$ or $HCOO^-$.

contrast to the $\Delta\Delta G^x$ values for the cationic/neutral metal complexes, the $\Delta\Delta G^x$ values for the *monoanionic* $\{[Zn\ (CH_3S)_3\ ImH]\cdot W\}^-$ complex (Table 3, last reaction) become negative when ϵ is ≥ 20 mainly because the solvation free energy gain of the *dianionic* $\{[Zn\ (CH_3S)_3\ ImH]\cdot HCOO\}^{2-}$ complex relative to that of the respective *monoanionic* $\{[Zn\ (CH_3S)_3\ ImH]\cdot CH_3CONHCH_3\}^-$ complex outweighs the greater cost of desolvating $HCOO^-$, as compared to $CH_3CONHCH_3$.

The results in Table 3 imply that the contribution of the second-shell Asp/Glu carboxylate to the Zn-core stability relative to that of the Bkb carbonyl depends on the net charge of the Zn complex and the solvent accessibility of the metal-binding site. Not surprisingly, a second-shell carboxylate stabilizes a *cationic*/*neutral* Zn-core more than an outer-shell $CH_3CONHCH_3$ in *buried* sites where metal−ligand electrostatic interactions are enhanced, but not in partially/fully solvent exposed sites where the favorable metal−ligand electrostatic interactions are attenuated and solute−solvent electrostatic interactions dominate. In fully solvent exposed sites, an outer-shell $CH_3CONHCH_3$ may not stabilize a *neutral* Zn-core (Table 3 footnotes f, h−j, positive ΔG^{80} for reactions 4a, 6a−8a). On the other hand, a second-shell carboxylate could stabilize an *anionic* Zn-core more than an outer-shell $CH_3CONHCH_3$ only in relatively solvent exposed sites (Table 3, negative $\Delta\Delta G^x$, $x \geq 20$, for the last reaction).

Effect of a Second-Shell Asp/Glu Carboxylate vs Bkb Carbonyl on the HOMO Energy of the Zn-Bound Hydroxide. Among the three most common catalytic Zn-cores, the Zn-bound water is thought to be deprotonated and to act as a nucleophile in the $[Zn\ \mathit{OH}\ (His)_3]^+$ and $[Zn\ \mathit{OH}\ (Asp/Glu)\ (His)_2]^0$ catalytic cores, whereas it undergoes exchange with an alcohol substrate in the $[Zn\ H_2O\ (Cys)_2\ His]^0$ core (see Figure 1). Thus, we studied the first two types of catalytic Zn-cores in the absence and presence of a second-shell Asp/Glu carboxylate or Bkb carbonyl to assess the contribution of the second-shell ligand in the Zn−His−[Bkb,Asp/Glu] triad in facilitating the Zn-bound hydroxide to undergo nucleophilic attack. To reveal how the outer-shell ligand affects the reactivity of the Zn-bound OH^-, we first compared the occupied molecular orbital (MO) energies of the $[Zn\ OH\ (ImH)_3]^+$ and $[Zn\ OH\ HCOO\ (ImH)_2]^0$ complexes with and without a second-shell $CH_3CONHCH_3$ and $HCOO^-$.

Figure 2a and 2b show that the high-energy end of the occupied MO energy spectrum for the $[Zn\ OH\ (ImH)_3]^+$ or $[Zn\ OH\ HCOO\ (ImH)_2]^0$ complex depends on the type of the Zn−His−[Bkb,Asp/Glu] triad. If a second-shell $CH_3CONHCH_3$ hydrogen bonds to a Zn-bound ImH, the occupied MO energy spectrum is similar to that in the corresponding Zn-complex without $CH_3CONHCH_3$. In particular, the HOMO energies of $\{[Zn\ OH\ (ImH)_3]\cdot CH_3CONHCH_3\}^+$ (−11.6 eV) and $\{[Zn\ OH\ HCOO\ (ImH)_2]\cdot CH_3CONHCH_3\}^0$ (−8.6 eV) are only slightly raised relative to that of $[Zn\ OH\ (ImH)_3]^+$ (−12.0 eV) and $[Zn\ OH\ HCOO\ (ImH)_2]^0$ (−9.2 eV). In contrast, when a second-shell $HCOO^-$ hydrogen bonds to a Zn-bound ImH, the occupied MO energy spectrum is dramatically raised relative to that in the corresponding Zn-complex without $HCOO^-$. Notably, the HOMO energies of $\{[Zn\ OH\ (ImH)_3]\cdot HCOO\}^0$ (−8.8 eV) and $\{[Zn\ OH\ HCOO\ (ImH)_2]\cdot HCOO\}^-$ (−5.6 eV) are significantly higher (less negative) than those of the respective Zn-complexes without a second-shell ligand or with a second-shell $CH_3CONHCH_3$. Hence, the negatively charged carboxylate group in the Zn−His−Asp/Glu triad elevates the HOMO energy of a cationic/neutral zinc core much more than the neutral carbonyl group in the Zn−His−Bkb triad, thereby facilitating the Zn-bound OH^- to attack the substrate.

Effect of a Second-Shell Asp/Glu Carboxylate vs Bkb Carbonyl on Electron Transfer and Redistribution from the Zn-Bound OH^- to an Electrophilic Substrate. To evaluate this effect, we computed global/local reactivity descriptors (see Calculations) for the Zn-bound hydroxide attack of CO_2 and the peptide Bkb, which model, respectively, the first step of the carbonic anhydrase and carboxypeptidase enzyme-catalyzed reactions (see Figure 1). The electron affinity (EA), ionization energy (IE), electronic chemical potential (μ), and hardness (η) of the electrophilic substrates (CO_2 and $CH_3CONHCH_3$) and the $[Zn\ OH\ (ImH)_3]^+$ and $[Zn\ OH\ HCOO\ (ImH)_2]^0$ complexes with and without a second-shell ligand are listed in Table 4. Note that the experimental EA, IE, μ, or η for the molecules in Table 4 are currently not available except for CO_2, whose measured values are close to the respective computed ones (see Table 1).

Table 4. Electronic Chemical Potential (μ), Hardness (η), the Stabilization Energy (ΔE) upon Transferring ΔN Electrons, and the Zn-bound Hydroxide Oxygen (O^H), Condensed Fukui Function (f^-), and Local Softness (s^-) in Model Catalytic Zinc Cores

	EA[a] (eV)	IE[b] (eV)	μ[c] (eV)	η[d] (eV)	ΔN[e] (e)	ΔE[f] (eV)	$f^-(O^H)$[g]	$s^-(O^H)$[h] (1/eV)
$\{[Zn\ OH\ (ImH)_3]\cdot Y\}^{1+n} + CO_2 \rightarrow$[i]								
CO_2	−1.52	14.85	−6.67	8.19				
$[Zn\ OH\ (ImH)_3]^+$	1.51	12.01	−6.76	5.25	0.00	0.000	0.25	0.024
$\{[Zn\ OH\ (ImH)_3]\cdot CH_3CONHCH_3\}^+$	1.17	11.64	−6.41	5.23	0.01	−0.001	0.52	0.050
$\{[Zn\ OH\ (ImH)_3]\cdot HCOO\}^0$	−0.61	8.82	−4.10	4.71	0.10	−0.127	0.77	0.082
$\{[Zn\ OH\ HCOO\ (ImH)_2]\cdot Y\}^{0+n} + CH_3CONHCH_3 \rightarrow$[i]								
$CH_3CONHCH_3$	−1.87	10.59	−4.36	6.23				
$[Zn\ OH\ HCOO\ (ImH)_2]^0$	−1.01	9.23	−4.11	5.12	0.01	−0.001	0.04	0.004
$\{[Zn\ OH\ HCOO\ (ImH)_2]\cdot CH_3CONHCH_3\}^0$	−1.14	8.56	−3.71	4.85	0.03	−0.009	0.19	0.019
$\{[Zn\ OH\ HCOO\ (ImH)_2]\cdot HCOO\}^-$	−2.96	5.57	−1.31	4.26	0.15	−0.222	0.23	0.027

[a] Computed from eq 12a at the MP2/6-31+G(d)//S-VWN/6-31+G(d) level. [b] Computed from eq 12b at the MP2/6-31+G(d)//S-VWN/6-31+G(d) level. [c] Computed from eq 1. [d] Computed from eq 2. [e] Computed from eq 4. [f] Computed from eq 5. [g] Computed from eq 10. [h] Computed from eq 11. [i] Y^n = $HCOO^-$ or $CH_3CONHCH_3{}^0$.

For both reactions in Table 4, a Zn-bound OH^- acts as the nucleophile to attack the electrophilic substrate (CO_2 or $CH_3CONHCH_3$). In the absence of a second-shell ligand, the electronic chemical potential of the *cationic* $[Zn\ OH\ (ImH)_3]^+$ complex (−6.8 eV) is slightly lower (more negative) than that of CO_2 (−6.7 eV), indicating that electrons are unlikely to flow from the Zn-bound hydroxide to the substrate (Table 4, ΔN = 0e). On the other hand, the electronic chemical potential of the *neutral* $[Zn\ OH\ HCOO\ (ImH)_2]^0$ complex (−4.1 eV) is higher (less negative) than that of $CH_3CONHCH_3$ (−4.4 eV), consistent with the direction of electron transfer in the enzymatic reaction from the Zn-bound hydroxide oxygen to the substrate's carbon atom (Table 4, ΔN = 0.01e).

The results in Table 4 show that the Zn−His−Bkb triad facilitates the Zn-bound OH^- of the $[Zn\ OH\ (His)_3]^+$ or $[Zn\ OH\ (Asp/Glu)\ (His)_2]^0$ catalytic core to attack the respective electrophilic substrate. The Zn−His−Bkb triad raises the electronic chemical potential of the $[Zn\ OH\ (ImH)_3]^+$ or $[Zn\ OH\ HCOO\ (ImH)_2]^0$ complex, thus increasing the number of electrons transferred to the substrate (by 0.01/0.02e) as well as the stabilization energy (by 0.02/0.18 kcal/mol), as compared to its absence. It also enhances the softness and reactivity of the Zn-bound hydroxide oxygen: The local softness, $s^-(O^H)$, and reactivity, $f^-(O^H)$, of the hydroxide oxygen in the $\{[Zn\ OH\ (ImH)_3]\cdot CH_3CONHCH_3\}^+$ or $\{[Zn\ OH\ HCOO\ (ImH)_2]\cdot CH_3CONHCH_3\}^0$ complex are greater than the respective values in the metal complex without the second-shell $CH_3CONHCH_3$.

The results in Table 4 also show that the Zn−His−Asp/Glu triad facilitates nucleophilic attack of the Zn-bound OH^- more than the Zn−His−Bkb triad, implying that it plays a more important catalytic role than the Zn−His−Bkb triad. The global/local reactivity descriptors are much more perturbed when the Zn-bound His interacts with a carboxylate group than when it interacts with a carbonyl group. The changes in electronic chemical potential (2.66/2.80 eV) and hardness (0.54/0.86 eV) of the reacting Zn-complex when it interacts with a second-shell $HCOO^-$ are significantly greater than the corresponding $\mu_B{}^0$ (0.35/0.40) and η_B (0.02/0.27 eV) changes when the same metal complex interacts with a second-shell $CH_3CONHCH_3$. These trends are also found when the global reactivity indices in Table 4 are computed using eq 12 or eq 13 at the B3-LYP/6-31+G*//B3-LYP/6-31+G* level (data not shown). Consequently, the Zn−His−Asp/Glu triad increases the number of electrons transferred (0.10/0.14e) and the stabilization energy (3 or 5 kcal/mol) much more than the Zn−His−Bkb triad (see above). It also increases the hydroxide oxygen's local softness more than the Zn−His−Bkb triad.

Table 5. Relative MP2/6-31+G(d) Energies (in kcal/mol) of the S-VWN/6-31+G(d) Fully Optimized Structures Resulting from Four Possible Bicarbonate Binding Modes

binding mode	structure	ΔE[a]
mono-OC	figure 3a	0.0
bi-OC	figure 3b	4.7
bi-OH	figure 3c	8.5
mono-OH	figure 3d	9.0

[a] Energy of the fully optimized structure starting from the binding mode listed in the first column relative to that of the fully optimized mono-OC structure in Figure 3a.

Effect of a Second-Shell Asp/Glu Carboxylate vs Bkb Carbonyl on Product Displacement by Water in Enzymatic Zinc Cavities. To investigate this effect, we calculated the free energy, ΔG^x, for displacing the Zn-bound product (HCO_3^-, CH_3COOH, or CH_3CHO) by a water molecule in Zn-complexes modeling the three most common types of catalytic Zn-cores (see Figure 1). In the $[Zn\ \mathit{HCO_3}\ (ImH)_3]^+$ complex the bicarbonate anion, HCO_3^-, could bind the Zn^{2+} cation in four possible binding modes: (1) one of the carboxylate oxygens monodentately bound (mono-OC, Figure 3a), (2) both carboxylate oxygens bidentately bound (bi-OC, Figure 3b), (3) one of the carboxylate oxygens and the hydroxyl oxygen bidentately bound (bi-OH, Figure 3c), or (4) the hydroxyl oxygen monodentately bound (mono-OH, Figure 3d). To identify the optimal binding mode, the $[Zn\ \mathit{HCO_3}\ (ImH)_3]^+$ structure was optimized starting from these four binding modes depicted in Figure 3a−d.

The results from the four possible binding modes in Table 5 and Figure 3a−d show that mono-OC binding to a tetracoordinated Zn^{2+} (Figure 3a) yields the lowest energy $[Zn\ \mathit{HCO_3}\ (ImH)_3]^+$ structure. Zn^{2+} prefers to be tetracoordinated rather than pentacoordinated, as the bidentate binding modes (bi-OC, Figure 3b, and bi-OH, Figure 3c) spontaneously convert to the mono-OC binding mode during S-VWN/6-31+G(d) geometry optimization. This is consistent with our previous finding that four-coordinate structures are lower in energy than five-coordinate structures.[61] Furthermore, Zn^{2+} prefers to bind monodentately to the carboxylate oxygen rather than to the

(54) Wolfenden, R.; Anderson, L.; Gullis, P. M.; Southgate, C. C. B. *Biochemistry* **1981**, *20*, 849−855.
(55) Wolfenden, R. *Biochemistry* **1978**, *17*, 201−204.
(56) Hine, J.; Mookerjee, P. K. *J. Org. Chem.* **1975**, *40*, 292−298.

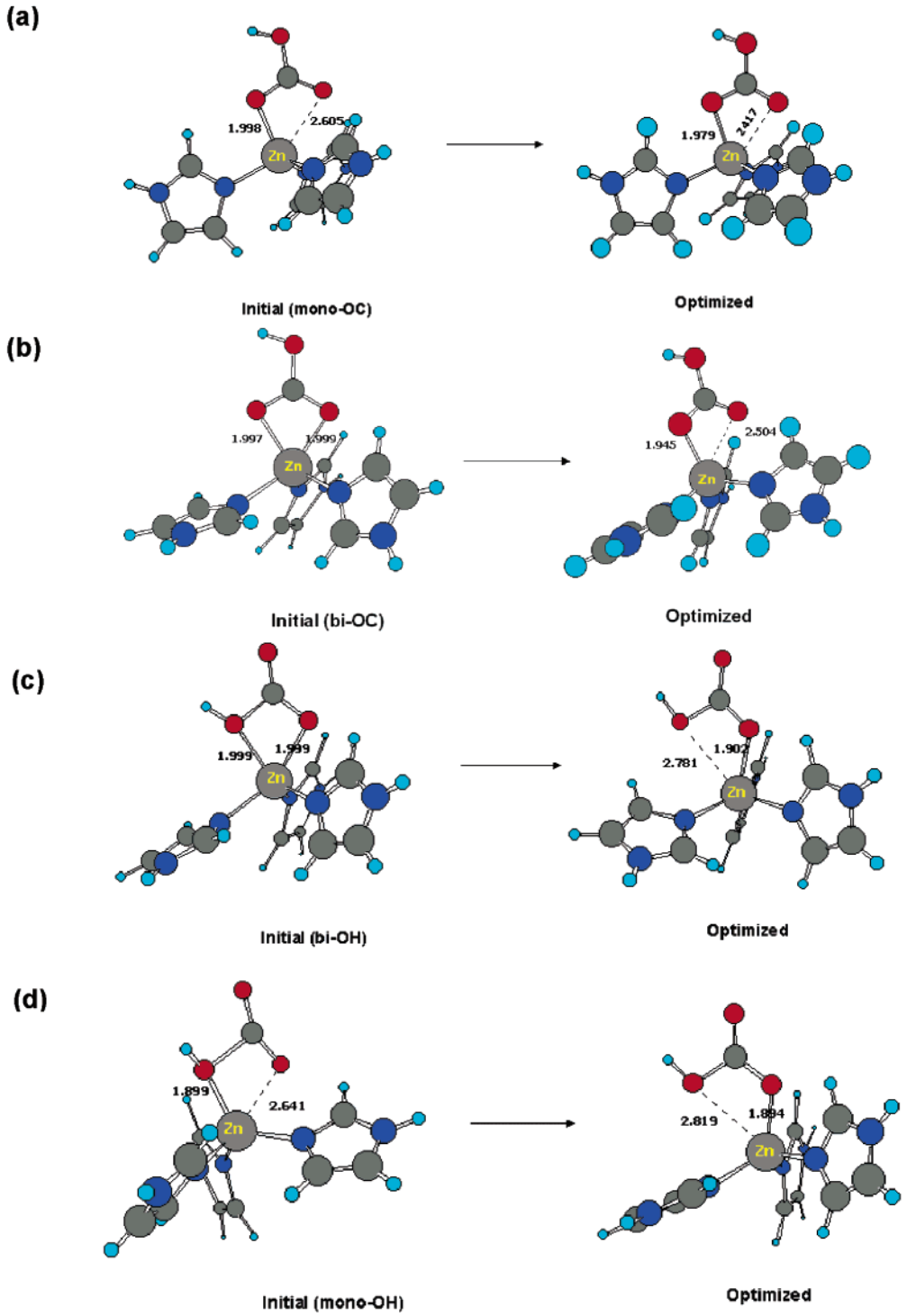

Figure 3. Fully optimized S-VWN/6-31+G(d) [Zn HCO_3 $(ImH)_3]^+$ structure starting from (a) one of the carboxylate oxygens monodentately bound to Zn^{2+} (mono-OC), (b) both carboxylate oxygens bidentately bound to Zn^{2+} (bi-OC), (c) one of the carboxylate oxygens and the hydroxyl oxygen bidentately bound to Zn^{2+} (bi-OH), and (d) the hydroxyl oxygen monodentately bound to Zn^{2+} (mono-OH).

hydroxyl oxygen, as the initial mono-OH binding mode (Figure 3d) spontaneously converts to the mono-OC binding mode during S-VWN/6-31+G(d) geometry optimization. The fully optimized structures resulting from the initial bi-OC, bi-OH, and mono-OH structures (Figure 3b−d) have higher MP2/6-31+G(d) energies than the fully optimized mono-OC structure in Figure 3a (by 4.7, 8.5, and 9.0 kcal/mol, respectively); thus the latter was used in computing the exchange free energies in Table 6.

(57) Pearson, R. G. *J. Am. Chem. Soc.* **1986**, *108*, 6109−6114.
(58) Bartmess, J. E.; McIver, R. T., Jr. *Gas-phase ion chemistry*; Academic Press: New York, 1979; Vol. 2.
(59) *Handbook of Physical Properties of Organic Chemicals*; Howard, P. H.; Meylan, W. M., Eds.; Lewis Publishers: Boca Raton, FL, 1997.
(60) Jencks, W. P.; Regenstein, J. *Handbook of Biochemistry and Molecular Biology*, 3rd ed.; CRC Press: Cleveland, OH, 1976; Vol. I.
(61) Dudev, T.; Lim, C. *J. Am. Chem. Soc.* **2000**, *122*, 11146−11153.

Table 6. Exchange Free Energies, ΔG^x, for $[X\ Z]^{m+n} + W \rightarrow [X\ W]^m + Z^n$ in Model Zinc-Sites of Different Dielectric Constant x[a]

reactants	products	$\Delta\Delta G^2$	$\Delta\Delta G^4$	$\Delta\Delta G^{20}$	$\Delta\Delta G^{80}$
$[X\ Z]^{m+n} + W$	$[X\ W]^m + HCO_3^-$				
1a. $[Zn\ \mathit{HCO_3}\ (ImH)_3]^+$	$[Zn\ W\ (ImH)_3]^{2+}$	0.0	0.0	0.0	0.0
1b. $\{[Zn\ \mathit{HCO_3}\ (ImH)_3]\cdot CH_3CONHCH_3\}^+$	$\{[Zn\ W\ (ImH)_3]\cdot CH_3CONHCH_3\}^{2+}$	−1.4[b]	1.8[b]	4.7[b]	5.4[b]
1c. $\{[Zn\ \mathit{HCO_3}\ (ImH)_3]\cdot HCOO\}^0$	$\{[Zn\ W\ (ImH)_2\ Im]\cdot HCOOH\}^+$	−29.9[b]	−8.7[b]	9.3[b]	13.2[b]
$[X\ Z]^{m+n} + W$	$[X\ W]^m + CH_3COOH$				
2a. $[Zn\ \mathit{CH_3COOH}\ HCOO\ (ImH)_2]^+$	$[Zn\ W\ HCOO\ (ImH)_2]^+$	0.0	0.0	0.0	0.0
2b. $\{[Zn\ \mathit{CH_3COOH}\ HCOO\ (ImH)_2]\cdot CH_3CONHCH_3\}^+$	$\{[Zn\ W\ HCOO\ (ImH)_2]\cdot CH_3CONHCH_3\}^+$	−1.8[c]	−1.7[c]	−1.8[c]	−1.9[c]
2c. $\{[Zn\ \mathit{CH_3COOH}\ HCOO\ (ImH)_2]\cdot HCOO\}^0$	$\{[Zn\ W\ HCOO\ ImH\ Im]\cdot HCOOH\}^0$	−12.9[c]	−7.7[c]	−2.4[c]	−1.1[c]
$[X\ Z]^m + n + W$	$[X\ W]^m + CH_3CHO$				
3a. $[Zn\ \mathit{CH_3CHO}\ (CH_3S)_2\ ImH]^0$	$[Zn\ W\ (CH_3S)_2\ ImH]^0$	0.0	0.0	0.0	0.0
3b. $\{[Zn\ \mathit{CH_3CHO}\ (CH_3S)_2\ ImH]\cdot CH_3CONHCH_3\}^0$	$\{[Zn\ W\ (CH_3S)_2\ ImH]\cdot CH_3CONHCH_3\}^0$	0.2[d]	0.9[d]	2.5[d]	3.1[d]
3c. $\{[Zn\ \mathit{CH_3CHO}\ (CH_3S)_2\ ImH]\cdot HCOO\}^-$	$\{[Zn\ W\ (CH_3S)_2\ ImH]\cdot HCOO\}^-$	−0.2[d]	1.1[d]	2.6[d]	3.2[d]

[a] See footnote a under Table 3. [b] Relative to the thermodynamic parameters of the respective reaction without a second-shell ligand, whose ΔG^2, ΔG^4, ΔG^{20}, and $\Delta G^{80} = 85.8$, 41.6, 4.8, and −2.7 kcal/mol, respectively. [c] Relative to the thermodynamic parameters of the respective reaction without a second-shell ligand, whose ΔG^2, ΔG^4, ΔG^{20}, and $\Delta G^{80} = 38.7$, 36.6, 34.2, and 33.6 kcal/mol, respectively. [d] Relative to the thermodynamic parameters of the respective reaction without a second-shell ligand, whose ΔG^2, ΔG,[4] ΔG^{20}, and $\Delta G^{80} = -1.8$, −2.3, −3.5, and -4.1 kcal/mol, respectively.

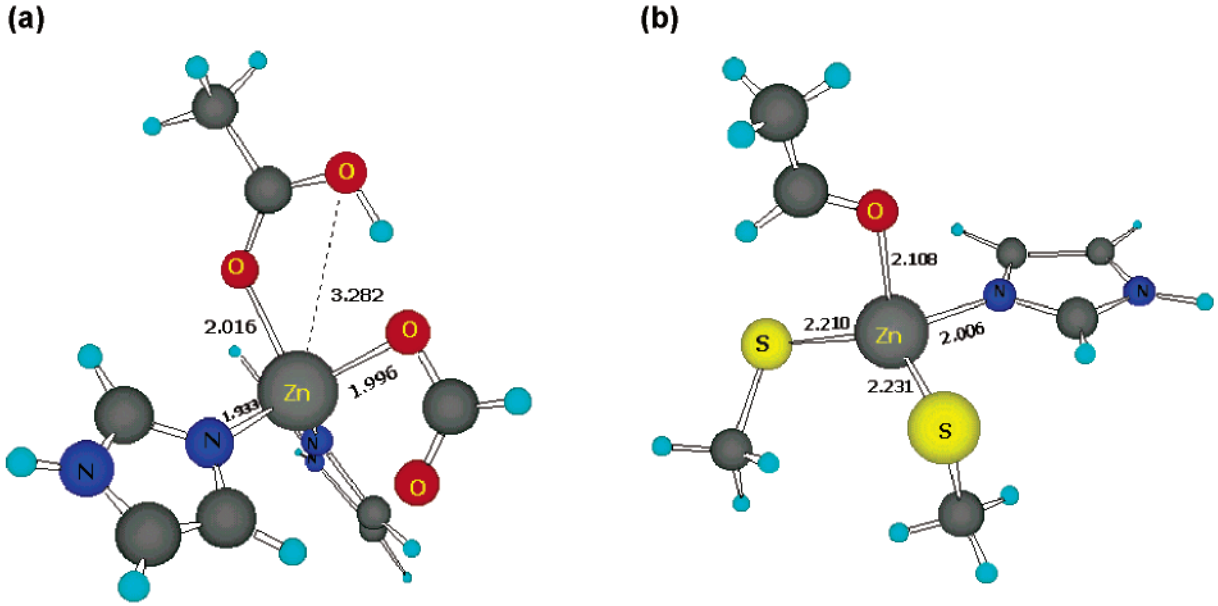

Figure 4. Fully optimized S-VWN/6-31+G(d) geometry of (a) $[Zn\ \mathit{CH_3COOH}\ HCOO\ (ImH)_2]^+$ and (b) $[Zn\ \mathit{CH_3CHO}\ (CH_3S)_2\ ImH]^0$.

As for the mono-OC $[Zn\ \mathit{HCO_3}\ (ImH)_3]^+$ structure, Zn^{2+} was assumed to be tetracoordinated and monodentately bound to the carbonyl oxygen in the $[Zn\ \mathit{CH_3COOH}\ HCOO\ (ImH)_2]^+$ and $[Zn\ \mathit{CH_3CHO}\ (CH_3S)_2\ ImH]^0$ complexes, whose fully optimized S-VWN/6-31+G(d) geometries are illustrated in Figure 4a and 4b, respectively. The other Zn^{2+} complexes in Table 6 were also *fully* optimized at the S-VWN/6-31+G(d) level. Note that in the *fully* optimized product geometries of reaction 1c, $\{[Zn\ W\ (ImH)_2\ Im]\cdot HCOO\mathit{H}\}^+$, and reaction 2c, $\{[Zn\ W\ HCOO\ ImH\ Im]\cdot HCOO\mathit{H}\}^0$, proton transfer to the outer-shell carboxylate is spontaneous, in accord with our previous work[32] and Table 3.

The product→H_2O exchange free energies in Zn-complexes containing a Zn−His−[Bkb] relative to those in the respective Zn-complexes without a second-shell ligand in Table 6 show that the Zn−His−Bkb triad does not seem to significantly facilitate the release of the Zn-bound product (HCO_3^-, CH_3COOH, or CH_3CHO). When a second-shell $CH_3CONHCH_3$ hydrogen bonds to a Zn-bound ImH, the product→H_2O exchange free energies ($\Delta\Delta G^x$, $x \geq 2$) relative to those for the respective Zn-complex without a second-shell ligand (Table 6, reactions 1b, 2b, and 3b) are either positive or within the error limits of the present calculations (±2 kcal/mol), indicating that the Zn−His−Bkb triad does not significantly aid product release from a buried or solvent exposed catalytic Zn-core.

The results in Table 6 also show that the Zn−His−[Asp/Glu] triad could facilitate the release of the Zn-bound product (HCO_3^- or CH_3COOH) depending on the type of catalytic Zn-core and its solvent exposure. As for the Zn−His−Bkb triad, the Zn−His−[Asp/Glu] triad does not seem to aid the release of CH_3CHO from a neutral $[Zn\ CH_3CHO\ (CH_3S)_2\ ImH]^0$ catalytic core (Table 6, positive $\Delta\Delta G^x$, $x > 2$, for reaction 3c). However, it facilitates the release of CH_3COOH from a monocationic $[Zn\ CH_3COOH\ HCOO\ (ImH)_2]^+$ catalytic core (Table 6, negative $\Delta\Delta G^x$, $x \geq 2$, for reaction 2c). On the other hand, the effect of the Zn−His−[Asp/Glu] triad on the release of HCO_3^- from a monocationic $[Zn\ HCO_3\ (ImH)_3]^+$ catalytic Zn-core is strongly dependent on its solvent exposure. In a buried site, the negatively charged carboxylate group stabilizes the dicationic product, $[Zn\ W\ (ImH)_3]^{2+}$, much more than the monocationic reactant, $[Zn\ HCO_3\ (ImH)_3]^+$, therefore facilitating the release of HCO_3^- (Table 6, negative $\Delta\Delta G^x$, $x \leq 4$, for reaction 1c). With increasing solvent exposure of the catalytic site, the presence of an outer-shell carboxylate group reduces

the net positive charge of the metal complex, and hence the desolvation penalty of the neutral reactant $\{[Zn\ HCO_3\ (ImH)_3]\cdot HCOO\}^0$ complex as well as the solvation free energy gain of the monocationic $\{[Zn\ W\ (ImH)_2Im]\cdot HCOOH\}^+$ complex, as compared to the respective complexes without a second-shell $HCOO^-$. The much smaller solvation free energy gain of the monocationic product complex relative to the respective dicationic complex without an outer-shell carboxylate group inhibits the release of HCO_3^- (Table 6, positive $\Delta\Delta G^x$, $x \geq 20$, for reaction 1c).

Discussion

Factors Governing the Relative Contributions of the Second-Shell Bkb Carbonyl and the Asp/Glu Carboxylate to the Zn-Core Stability. The results in Table 3 show that the relative contributions of the second-shell Bkb carbonyl and the Asp/Glu carboxylate to the Zn-core stability depend mainly on (1) the solvent accessibility of the Zn-site and (2) the composition of the Zn-core, which determines the net charge of the Zn-complex. In deeply *buried* sites where electrostatic interactions between the second-shell ligand and the Zn-core are enhanced, a negatively charged carboxylate group stabilizes a *cationic*/*neutral* Zn-core (through favorable charge−charge/charge−dipole interactions) more than a neutral carbonyl group (dipole−charge/dipole−dipole interactions) (Table 3, negative $\Delta\Delta G^x$, $x \leq 4$, for reactions 1b−8b), whereas the latter stabilizes an *anionic* Zn-core (through dipole−charge interactions) more than the former (repulsive negative charge−negative charge interactions) (Table 3, positive $\Delta\Delta G^x$, $x \leq 4$, for reaction 9b). On the other hand, in partially/fully *solvent-exposed* sites both the second-shell Bkb carbonyl and Asp/Glu carboxylate in the Zn−His−[Bkb,Asp/Glu] triad do not seem to stabilize *cationic*/*neutral* Zn-cores (Table 3, generally positive $H_2O \rightarrow HCOO^-$/$CH_3CONHCH_3$ ΔG^x, $x \geq 20$), but they could stabilize *anionic* Zn-cores (Table 3, negative ΔG^x, $x \geq 20$, for reactions 9a and 9b).

Advantage of a Second-Shell Bkb Carbonyl over an Asp/Glu Carboxylate in *Structural* Zn Sites. A PDB survey[19] of nonredundant Zn-containing proteins shows that most of the structural Zn sites are relatively buried with solvent accessible surface areas (SASA) less than 30%,[62] typically characterized by [Zn $(Cys)_4$], [Zn $(Cys)_3$ (His)], and [Zn $(Cys)_2$ $(His)_2$] cores with net charges of −2, −1 and 0, respectively. However, not all *structural* Zn sites are buried, as some contain water molecule(s) in the metal's first or second coordination shell. Interestingly, 10 of the 75 *structural* Zn sites contain the Zn−His−*Bkb* triad with net charges of −1, 0, or +1, while only 2 *nonanionic* sites contain the Zn−His−[*Asp*/*Glu*] triad (PDB entries: 1AU1 and 1CLC).

The empirical observation that the Bkb carbonyl group, rather than the Asp/Glu carboxylate side chain, is the most common partner of the Zn-bound His in *structural* Zn sites is generally consistent with the results in Table 3: The Zn−His−*Bkb* triad is predicted to stabilize *anionic*, *buried* Zn-cores or *nonanionic*, *solvent-exposed* Zn-cores more than the corresponding Zn−His−[*Asp*/*Glu*] triad (Table 3). This is consistent with the finding that the *structural* Zn sites containing the Zn−His−*Bkb* triad are either *anionic* ([Zn $(Cys)_3$ $(His)]^-$) and *buried* (PDB entries: 1BTK, 1PTQ, 1PUD, and 1ZFO) or *nonanionic* ([Zn $(His)_x$ $(Asp/Glu)_y$ $(H_2O)_{4-x-y}]^{+/0}$, $x = 1-3$; $y = 1$ or 2, and [Zn $(Cys)_2$ $(His)_2]^0$) and accessible to water molecules (PDB entries: 1E7O, 1SLN, 1STE, and 1GUQ), except the buried [Zn $(Cys)_2$ $(His)_2]^0$ site in the nuclear factor (PDB entry 1FRE; see below).

On the other hand, the absence of the Zn−His−[*Asp*/*Glu*] triad in certain *buried* [Zn $(Cys)_2$ $(His)_2]^0$ sites seems inconsistent with the prediction that the Zn−His−[*Asp*/*Glu*] triad stabilizes *neutral*, *buried* Zn-cores such as [Zn $(Cys)_2$ $(His)_2]^0$ more than the respective Zn−His−*Bkb* triad (Table 3, negative $\Delta\Delta G^x$, $x \leq 4$, for reaction 8b). One possible explanation stems from the observation that, in some Zn-finger proteins such as the Zif268 Zn-finger peptide (PDB entry, 1AAY) and the tramtrack protein (PDB entry, 2DRP), a Zn-bound His is found to interact with DNA. Hence, a neutral second-shell Bkb or water molecule would presumably stabilize the protein−DNA interface more than the respective negatively charged Asp/Glu. This is in accord with the hypothesis in our previous work that a DNA-binding site is generally located in an unfavorable electrostatic environment in the absence of stabilizing electrostatic interactions from the negatively charged DNA.[63]

Advantage of a Second-Shell Asp/Glu Carboxylate over a Bkb Carbonyl in Catalytic Zn Sites. A PDB survey of Zn-proteins[19] shows that the *common catalytic* Zn sites are *buried* with average SASA less than 10% for the Zn-binding residues (4% for carboxypeptidase A, PDB entry 2CTC and 5% for alcohol dehydrogenase, PDB entry 2OHX).[19] It also shows that *mononuclear catalytic* Zn sites containing the Zn−His−[Bkb, Asp/Glu] triad are either positively charged or neutral and the Zn−His−Asp/Glu triad is found more often than the Zn−His−Bkb triad.[19] Our previous work showed that the Asp/Glu side chain in the Zn−His−Asp/Glu triad can increase the negative charge of its partner, His, and create an anionic hole that may stabilize a *buried*, *cationic*/*neutral* Zn-complex.[32] This suggests an *indirect* role for the Zn−His−Asp/Glu triad in catalysis as the three most common catalytic Zn-cores, depicted in Figure 1, are either *positively charged* or *neutral*. However, there has been no concrete evidence for a direct role of the Zn−His−Asp/Glu or the Zn−His−Bkb triad in catalysis.

The calculations herein reveal the different effects of the Zn−His−Asp/Glu vs the Zn−His−Bkb triad on the Zn-core reactivity during the course of the enzyme-catalyzed reaction, thus explaining why the Zn−His−Asp/Glu triad is found more often than the Zn−His−Bkb triad in catalytic Zn sites. The Zn−His−Asp/Glu stabilizes buried cationic/neutral *catalytic* Zn sites more than the Zn−His−Bkb triad regardless of whether the zinc-bound water molecule is protonated or deprotonated (Table 3, negative $\Delta\Delta G^x$, $x \leq 4$, for reactions 1b−7b). The negatively charged carboxylate side chain in the Zn−His−Asp/Glu triad enhances the reactivity of the [Zn OH $(His)_3]^+$ or [Zn OH (Asp/Glu) $(His)_2]^0$ catalytic cores more than the neutral carbonyl group in the Zn−His−Bkb triad by increasing (i) the HOMO energy of the cationic/neutral zinc core, (ii) the reactivity of the attacking Zn-bound OH^-, (iii) electron transfer to the substrate, and (iv) the stability of the metal complex upon electron transfer (see Table 4). Furthermore, it facilitates the release of the Zn-bound product (HCO_3^- or CH_3COOH) from

(62) Gromiha, M. M.; Oobatake, M.; Kono, H.; Uedaira, H.; Sarai, A. *Protein Eng.* **1999**, *12*, 549−555.

(63) Chen, Y. C.; Wu, C. Y.; Lim, C. In preparation.

relatively *buried*, *monocationic* [Zn HCO_3 $(His)_3]^+$ or [Zn CH_3-COOH (Asp/Glu) $(His)_2]^+$ catalytic cores more than the neutral carbonyl group in the Zn−His−Bkb triad (Table 6, $\Delta\Delta G^x$, $x \leq 4$, for reactions 1c and 2c are more negative than those for reactions 1b and 2b, respectively). This is mainly because, in buried sites, the $Zn^{\delta+}\cdots Im^{\delta-}\cdots HCOOH^{\mu}$ charge−charge−dipole interactions in the $\{[Zn\ W\ (ImH)_2\ Im]\cdot HCOOH\}^+$ and $\{[Zn\ W\ HCOO\ ImH\ Im]\cdot HCOOH\}^0$ products are more favorable than the $Zn^{\delta+}\cdots ImH^{\mu}\cdots CH_3CONHCH_3^{\mu}$ charge−dipole−dipole interaction in the corresponding $\{[Zn\ W\ (ImH)_3]\cdot CH_3CONHCH_3\}^{2+}$ and $\{[Zn\ W\ HCOO\ (ImH)_2]\cdot CH_3CONHCH_3\}^+$ products.

Acknowledgment. We thank Dr. T. Dudev and I. Tunnel for helpful discussions. We are grateful to Drs. D. Bashford, M. Sommer, and M. Karplus for the program to solve the Poisson equation. This work was supported by the National Science Council, Taiwan (NSC Contract No. 91-2311-B-001), the Institute of Biomedical Sciences, and the National Center for High-Performance Computing, Taiwan.

Supporting Information Available: Complete refs 29 and 42. This material is available free of charge via the Internet at http://pubs.acs.org.

JA051304U